Research Article **Open Access**

O. Idigoras, E. Nikulina, J. M. Porro, P. Vavassori, A. Chuvilin, A. Berger*

FEBID fabrication and magnetic characterization of individual nano-scale and micro-scale Co structures

Abstract: This work gives an illustration of the viability of FEBID to fabricate magnetic nano- and micro-structures and it demonstrates that by means of a combination of MOKE microscopy and MFM, one is able to analyze the size and shape effects in individual magnetic cobalt structures. With the help of our magnetic and functional study, we are able to demonstrate that by using FEBID, cobalt of uniform thickness and magnetic response can be deposited over several micron-size areas, establishing a most crucial ingredient of reliable structure and device fabrication. Furthermore, we show the suitability of FEBID to fabricate functional and complex 3-dimensional magnetic structures. The issue of unintended secondary deposits in FEBID is discussed, and a Xe-ion milling post-treatment for its removal is proposed and demonstrated as a successful pathway towards the fabrication of functionally independent magnetic nano-structures.

Keywords: nanofabrication, magnetization reversal

Doi: 10.2478/nanofab-2014-0003
received February 27, 2014; accepted May 06, 2014

1 Introduction

Technological advances today are demanding an ever-increasing integration and further miniaturization of devices, especially in the electronics industry. Among such devices, ferromagnetic systems have important technological relevance, primarily in the data storage industry [1], for magnetic sensors [2] and logic gates [3]. Hereby, the continuously more challenging demands of technology and the need to understand the fundamental physics, upon which this technology is based, have made the study of magnetization reversal in nanoscale dimensions a core area of active research during the last decade [4-12]. This relevance is further extended by recent key discoveries, such as current- and voltage-induced phenomena in nano-scale ferromagnets [13,14], which enable completely new device concepts like the magnetic race-track memory [15].

Despite the large number of efforts in this field, there are still many open questions that need to be addressed, such as the precise understanding of magnetization reversal in individual structures. On the other hand, in order to miniaturize ferromagnetic systems, it is essential to find efficient pathways of fabricating such structures with the desired properties and to be able to characterize their individual magnetic properties with sufficient detail and precision. Also, in terms of technological bottlenecks, efficient and reliable pathways for 3-dimensional structure fabrication are yet to be found.

During the last few years, the focused electron beam induced deposition (FEBID) technique has been proposed and developed as an alternative to other multi-step lithography techniques [16–18]. The main reasons why FEBID is becoming a promising technique for nanofabrication are: (I) simplicity, since it is a one-step technique, (II) ability to fabricate structures with sizes even below 1 nm [19] and (III) the possibility to create geometrically complex structures, including non-trivial 3-dimentional entities [20,21].

Among the elemental ferromagnetic materials that can be deposited by FEBID, cobalt (Co) is particularly promising, because the achievable purities are exceptionally high, up to 95 at. % [22,23], and functional deposits with lateral sizes down to 30 nm have been demonstrated [10,22]. Due to these promising characteristics, studies have been performed that demonstrate the viability to fabricate

***Corresponding author: A. Berger:** CIC nanoGUNE Consolider, Tolosa Hiribidea 76, E-20018 Donostia-San Sebastian, Spain, e-mail: a.berger@nanogune.eu
O. Idigoras, E. Nikulina, J. M. Porro, P. Vavassori, A. Chuvilin: CIC nanoGUNE Consolider, Tolosa Hiribidea 76, E-20018 Donostia-San Sebastian, Spain
P. Vavassori, A. Chuvilin: Ikerbasque, Basque Foundation for Science, E-48011 Bilbao, Spain

functional Co structures with FEBID, such as, nano-Hall sensors [22,24], magnetic force microscopy tips [20,25] and domain wall conduits [26].

For the purpose of studying magnetization reversal of individual micro- and nano-structures, Magneto-Optical Kerr Effect (MOKE) microscopy has been shown to be a very efficient and sensitive method that enables the measurement of the magnetization reversal behavior in structures that are far smaller than the optical resolution limit [10,27,28].

2 Experimental procedure

The FEBID technique utilizes a highly focused electron beam for the purpose of fabricating nano-structures (Figure 1 (a)). The methodology itself is based on the decomposition of a suitable gaseous precursor, for example $Co_2(CO)_8$ for Co deposition, into volatile and nonvolatile components through electron-impact dissociation by the secondary electrons that are locally generated by the highly focused electron beam. While the volatile component, CO in the case of $Co_2(CO)_8$, desorbs, the nonvolatile component forms a deposit on the substrate. Correspondingly, material is deposited in the region that the primary electron beam has irradiated. Provided that one has positioning control for the focused primary beam, any arbitrarily shaped surface structure can be fabricated in one step. Thus, FEBID utilizes a principle that is somewhat similar to 3D-printing and allows for the fabrication of 3D structures. Modern double beam (Focused Ion Beam) FIB/(Scanning Electron Microscope) SEM instruments contain by default all the components necessary to realize the FEBID process: a high resolution electron column forming a highly focused electron beam in a broad range of energies and currents, a Gas Injection System (GIS) supplying a flow of precursor gas directly onto the deposition area, a high precision sample stage with at least 5 degrees of freedom, a high resolution fast digital scan generator, and a patterning engine for precise control over the beam positioning. In our work we have used a Helios 600 Nanolab DualBeam system (FEI Company). Figure 1 (b) shows as an example an array of Co nanopillars fabricated by FEBID via a grid-pattern electron beam exposure.

In order to characterize the magnetization reversal of the Co structures fabricated by FEBID, we have used a MOKE microscope from EVICO Magnetics GmbH [29,30]. In MOKE microscopy, the magnetic state of a structure is measured by means of analyzing the polarization change of light reflected from the surface via a suitable optical microscope. For this purpose, the light emitted from a high-intensity lamp is converted into linearly polarized light that is used to evenly illuminate the sample surface (see Figure 2). After reflection, the light is passed through a combination of compensator and analyzer, so that the subsequent light intensity is proportional to the Kerr effect and therefore, dependent on the sample magnetization state. The light itself is recorded by a CCD-camera to allow for laterally resolved detection in conjunction with the microscope objective, from which one can obtain the magnetic image after subtracting the non-magnetic background. In all experiments shown here, the MOKE signal is sensitive to the magnetization component parallel to H.

In addition to domain imaging with an optical microscopy resolution limit of approximately 500 nm, our Kerr microscope allows the measurement of local magnetization M versus applied field H curves by

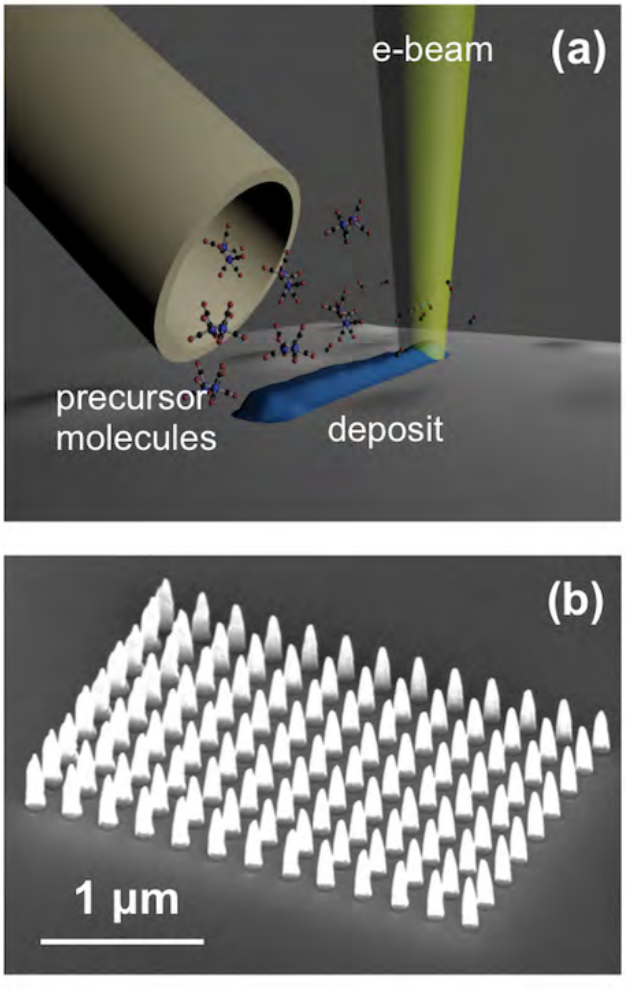

Figure 1: (a) Schematic of the electron beam induced deposition process; (b) scanning electron microscope image of a Co nanopillar matrix that was fabricated by FEBID.

following the light intensity signal as a function of *H*. Figure 3 shows an example of such an *M(H)* curve and associated domain images performed on a focused ion beam fabricated Co/Pt multilayer nanostructure that is 0.5 µm x 5 µm in size. While Figure 3 (a) shows an area-averaged signal integrated over 5 hysteresis loops for perpendicular applied field orientation with respect to the sample surface, Figures 3 (b)-(d) display domain images taken at different states along an individual magnetization reversal process. Different grey scales in the image represent different magnetization orientations. While (b) and (d) show uniform magnetic states of opposite orientation, (c) shows the type of multi-domain state that occurs right in the midst of the magnetization reversal process.

Hereby, it is an important experimental aspect to notice that while recording hysteresis loops, i.e. the cyclical *M(H)* dependence, one can measure the signal of the entire CCD camera image or collect the signal of only part of the CCD array. Specifically, our microscope has the flexibility to record the signal of any subsection of the CCD array by selecting any arbitrarily shaped area, in which the signal is integrated, and which we call the region of interest (ROI). By doing so, one can analyze the hysteresis loop signal of small areas or sample subsections by pre-selecting only the most suitable or interesting pixels in the ROI. In a previous work we have demonstrated that this makes it possible to measure magnetization reversal of only 30 nm wide individual Co wires, i.e. wires that are far smaller than the optical diffraction limit [10]. This is possible, because the microscope allows one to minimize the intensity coming from the non-magnetic sample part, which would add excessive noise to the integrated signal and correspondingly reduce the signal-to-noise ratio. As an example, Figure 4 shows a single cycle hysteresis loop measurement performed on a 30 nm wide FEBID-

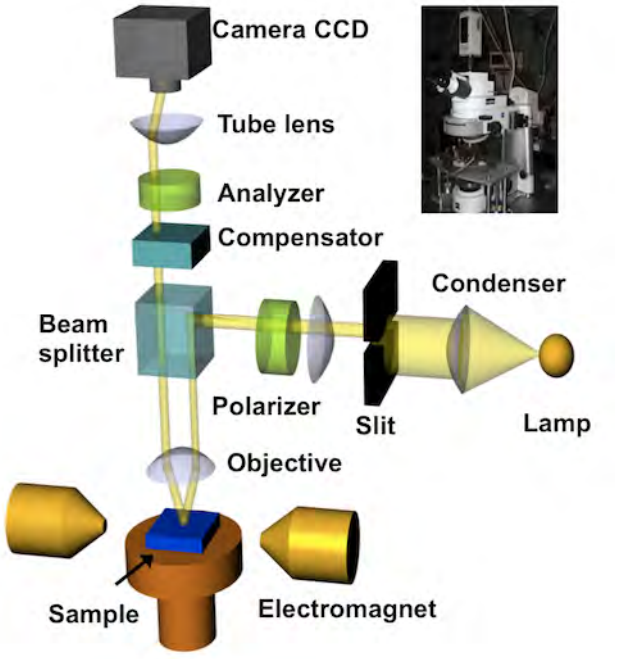

Figure 2: Schematic of our magneto-optical Kerr effect microscope; the inset shows a photograph of the actual microscope system.

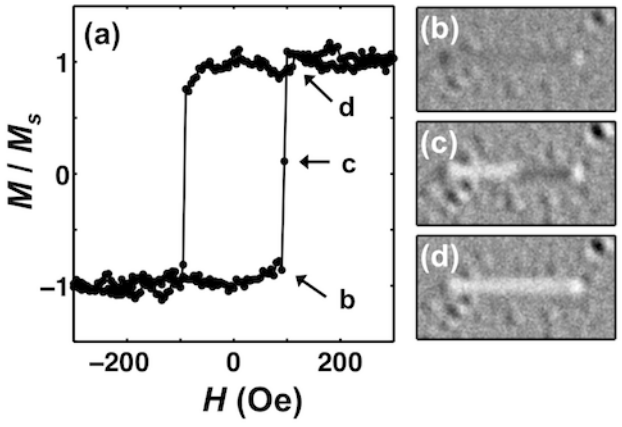

Figure 3: Magneto-optical characterization of a focused ion beam fabricated Co/Pt multilayer nanostructure that is 0.5 µm x 5 µm in size; (a) shows the *M*(*H*)-signal trace averaged over 5 hysteresis loops. (b)-(d) are domain images taken at different states along the magnetization reversal path. While (b) and (d) show uniform magnetic states, (c) shows an intermediate multi-domain state.

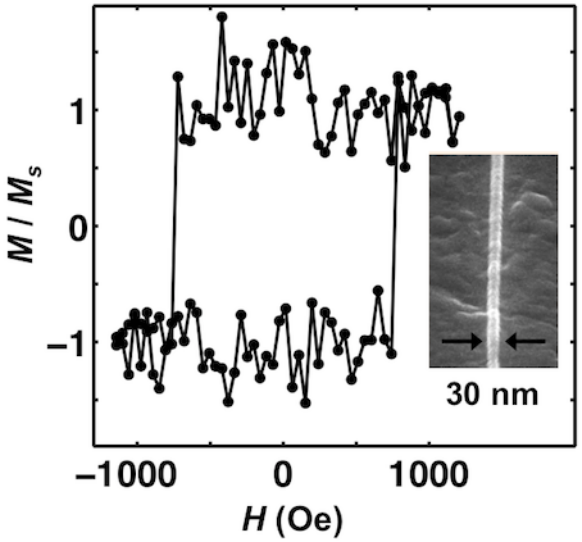

Figure 4: Single cycle hysteresis loop measurement for a 30 nm wide FEBID Co wire that was acquired by means of magneto-optical Kerr effect microscopy; the inset shows a scanning electron microscope image of the wire. Results reprinted with permission from E. Nikulina, O. Idigoras, P. Vavassori, A. Chuvilin and A. Berger, Appl. Phys. Lett. **100**, 142401 (2012). Copyright 2012, AIP Publishing LLC.

fabricated Co wire, while the inset in Figure 4 displays an SEM image of this wire.

Another technique we use here to characterize the magnetic properties and states of our structures is Magnetic Force Microscopy (MFM) [31]. This technique is a variation of atomic force microscopy and is based on the magnetic dipole-dipole interaction between a magnetic tip and a magnetic sample. Basically, the MFM methodology consists of scanning a sharp magnetic tip over a magnetic sample and measuring the locally varying magnetic dipole-dipole interaction through the corresponding deflection of the tip cantilever. By following the probe trace of the cantilever, one is able to image the magnetic field pattern above the sample surface, which is indicative of the magnetic domain structure in the ferromagnetic sample itself. To be able to separate this magnetic tip-sample interaction from the topographic structure, one must first acquire a topographic image of the surface in close proximity and then perform a second scan using the topographic data to maintain a fixed and slightly larger distance between the tip and surface. In this way, the contrast of this secondary scan is dominated by magnetic forces. In the MFM measurements shown for FEBID Co structures, we used an interleave distance of 90 nm. Figure 5 shows a schematic of the technique, while the inset Figure shows an MFM scan picture of a magnetic stripe domain structure that was measured for a 200 nm thick Co film with perpendicular magnetic anisotropy. This thick Co film has been epitaxially grown with (0001) crystallographic orientation by means of sputter deposition in an ultra high vacuum multi-chamber system.

3 Results

A scanning electron microscopy image of some of the FEBID structures fabricated and studied in this work is shown in Figure 6 (a). Specifically, these FEBID structures are Co rectangles of 5 µm length and different widths, namely 1 µm, 2 µm and 5 µm. For the fabrication process of these rectangles, the electron beam conditions have been set to 30 kV of beam energy and 2.7 nA of beam current. The dwell time and pitch size were 1 µs and 5 nm respectively, while the base pressure was 2×10^{-4} Pa. The average precursor pressure in the chamber was 1×10^{-3} Pa, which resulted in a precursor flux on the surface of the sample of approximately 10000 molecules/($nm^2 \cdot s$) considering the specific configuration of our experimental system. EDX measurements of structures grown under the same conditions showed a Co content higher than 80 at. %. All FEBID structures shown in this work have been deposited onto natively oxidized silicon wafers, which were previously cleaned by means of acetone and isopropanol in an ultrasonic bath. Figure 6 (b) shows the same structures imaged with the optical microscope that is being utilized for the MOKE microscopy studies, but without polarization contrast. While such structures are rather large in comparison to many technologically relevant devices today, they are nonetheless very helpful in studying the quality of FEBID deposits, because the physical structures here are of the same size as the typical micromagnetic domain structures that occur in ferromagnets [32-34]. Thus, the ideal behavior of micron size elements is

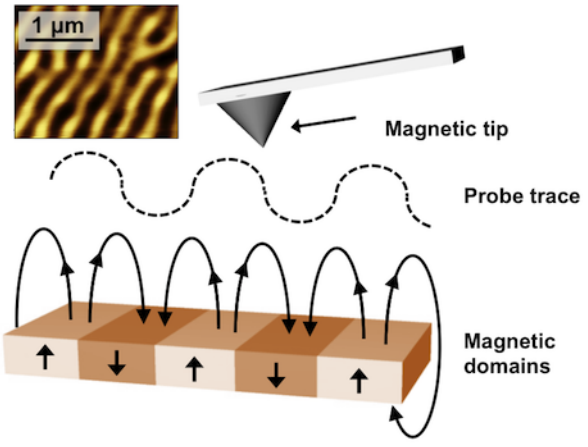

Figure 5: Schematic of magnetic force microscopy; the inset Figure corresponds to a magnetic force microscopy image of a 200 nm thick sputtered Co film exhibiting a perpendicular magnetic stripe domain structure.

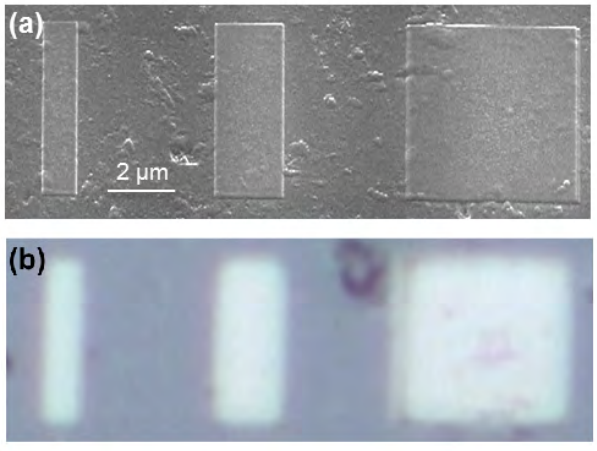

Figure 6: Scanning electron microscope (a) and optical microscope (b) images of rectangular shaped FEBID Co structures with 5 µm length and 1 µm, 2 µm and 5 µm widths, respectively. Results reprinted with permission from E. Nikulina, O. Idigoras, P. Vavassori, A. Chuvilin and A. Berger, Appl. Phys. Lett. **100**, 142401 (2012). Copyright 2012, AIP Publishing LLC.

well-known and understood, but it only occurs if the fabrication process indeed produces films of uniform thickness, uniform magnetic properties and is made from a material that has strong and uniform inter-granular exchange coupling. Otherwise, micron size collective magnetization behavior cannot build-up and one observes a magnetic pattern and magnetic response that is simply an area average of locally disjoined ferromagnetic nano-crystals.

Hysteresis loops recorded by means of MOKE microscopy in different regions of the 5 µm x 5 µm structure can be seen in Figure 7. The inset Figures represent the selected ROIs that were used to record each of the hysteresis loops by dashed red lines on top of the optical sample image. The hysteresis loop that is measured for the entire structure (Figure 7 (a)) shows non-hysteretic behavior due to the fact that the flux closure domain structure that exists in such square pattern of sufficient size can always accommodate the changing magnetic field strength and hereby find the global energy minimum, as schematically indicated in Figure 7 (d). However, as one can also see from the schematic, not all parts of the sample will react in an equal fashion to the applied field, so locally the hysteresis response can be very different. This is shown experimentally in Figures 7 (b) and (c). Here, we observe that if one places a horizontally oriented rectangular ROI on one of the edges that is aligned with the applied field and magnetization detection orientation, a hysteresis loop is visible (Figure 7 (b)). On the other hand, when placing a vertically oriented rectangular ROI on one of the edges that is perpendicular to the applied field orientation, hysteretic behavior is absent again. This difference in behavior can be easily understood with the help of the two schematics in Figure 7 (d) representing domain configurations at remanence and at modest applied field strength along the horizontal axis. As mentioned before, at remanence the system exhibits a flux closure domain structure (left hand side image in Figure 7 (d)), which is formed in order to minimize the magnetostatic energy. As a result of this flux closure domain formation, the remanent magnetization of the entire structure is zero. However if one analyzes the magnetization on the bottom edge of the structure individually as is the case of the hysteresis loop shown in Figure 7 (b), a non-vanishing remanent value is observed. The same type of behavior, but in reverse orientation, is found by analyzing the *M(H)* behavior on the top edge of the structure. If one places the ROI on the left or right edge of the system, the magnetization projection along the applied field direction at zero field is vanishing, due the orthogonal orientation of the magnetization vector with respect to the applied

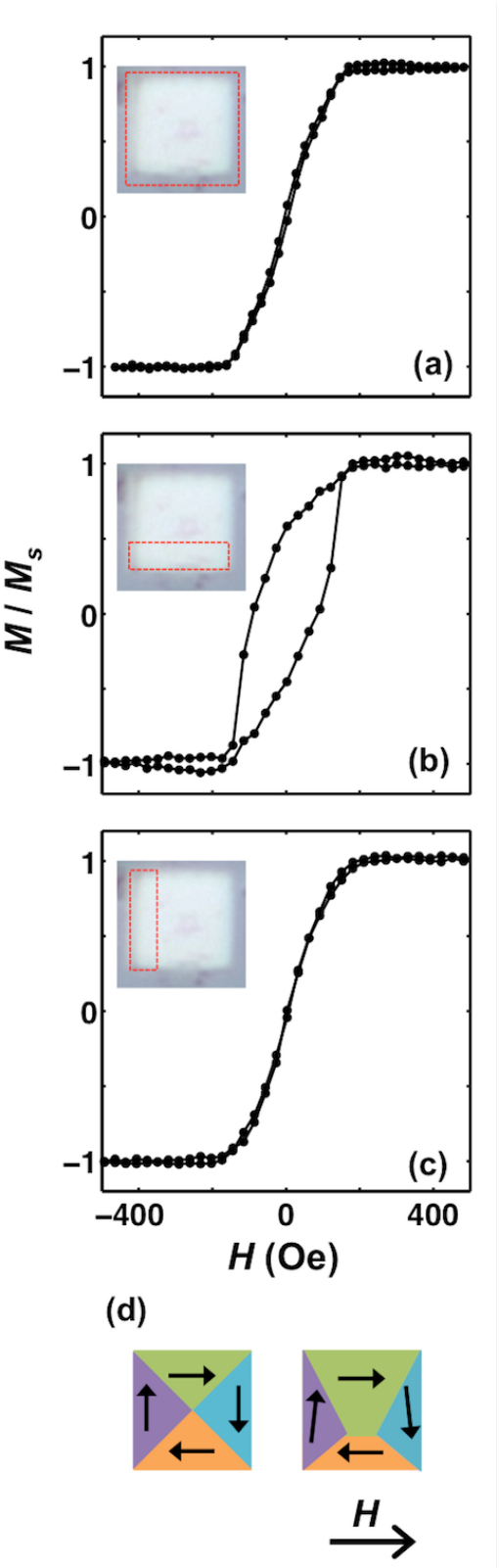

Figure 7: (a)-(c) Hysteresis loops measured on the 5 µm x 5 µm FEBID Co structure for different regions of interest; the inset Figures in (a)-(c) show the selected region of interest in each case. (d) displays schematic representations of the domain structure in remanence and for a small field applied along the horizontal axis.

field direction. Thus the remanent magnetization is zero as observed experimentally in Figure 7 (c). Upon applying an external field the flux closure domain is shifted and becomes asymmetric, which can be seen on the right hand side image in Figure 7 (d). The domain with the magnetization parallel to the externally applied field increases in size via domain wall movement, while the anti-parallel oriented domain shrinks. Nonetheless, it takes a certain level of field strength to move the domain wall all the way to the bottom or top of the structure. Thus, the regions near the upper and lower edges appear initially unperturbed by anti-parallel magnetic fields, so that a hysteretic local field dependence occurs as seen in Figure 7 (b). The domains with magnetization orientations pointing perpendicular to the external field on the left and right edges of the structure simply rotate towards the field direction upon applying a field, which is reversible and thus hysteresis free.

A slightly different magnetization reversal behavior is observed for the rectangular shaped structure that is 5 µm x 2 µm in size. Figure 8 shows two hysteresis loops measured for this structure, for which the field was applied parallel to the long (Figure 8 (a)) and short axes (Figure 8 (b)), respectively. The left-hand insets in both Figures represent the selected ROI that was used to measure these hysteresis loops by red dashed lines on top of the optical sample image. Here, identical ROI have been used to measure the overall magnetic response in both cases. Nonetheless, there are key differences between these two measurements that are due to the different size and shape of the sample in comparison to the 5 µm x 5 µm structure of Figure 7. The first difference is that the structure is smaller, so that domain structures have less space to build up and arrange in a way to minimize the overall magnetic energy [32]. The second aspect, which is even more obvious, is that this structure has reduced symmetry and long and short axes are distinctively different. Correspondingly, the magnetization reversal behavior is modified and anisotropic here. If the external field is applied parallel to the long axis, we observe the remanent magnetization to be zero and no hysteresis being present in central portion of the hysteresis loop, just as in the case of 5 µm x 5 µm structure. However, we also find two hysteretic segments in the loop that occur at field strengths in between 50 Oe and 100 Oe, which did not existent in the quadratic 5 µm x 5 µm structure. The pinching of the hysteresis loop, i.e. the absence of hysteresis at remanence, is the result of a flux closure domain structure, which is visualized by means of the MFM image taken in the remanent state (inset Figure 8 (a)). In order to initiate this domain formation upon coming from large applied field values, however, the activation energy for the domain nucleation has to be overcome. Given the changed size and shape of this structure, this nucleation does not occur in thermal equilibrium, but becomes only feasible at a slightly shifted applied field value, which has the observed hysteretic behavior as its net effect. When applying the external field along the short axis of the structure, the *M(H)* curve shows virtually no hysteretic behavior. This is due to the fact that the magnetostatic energy of this geometric hard axis magnetized state is higher and correspondingly triggers the domain nucleation more easily. The increase

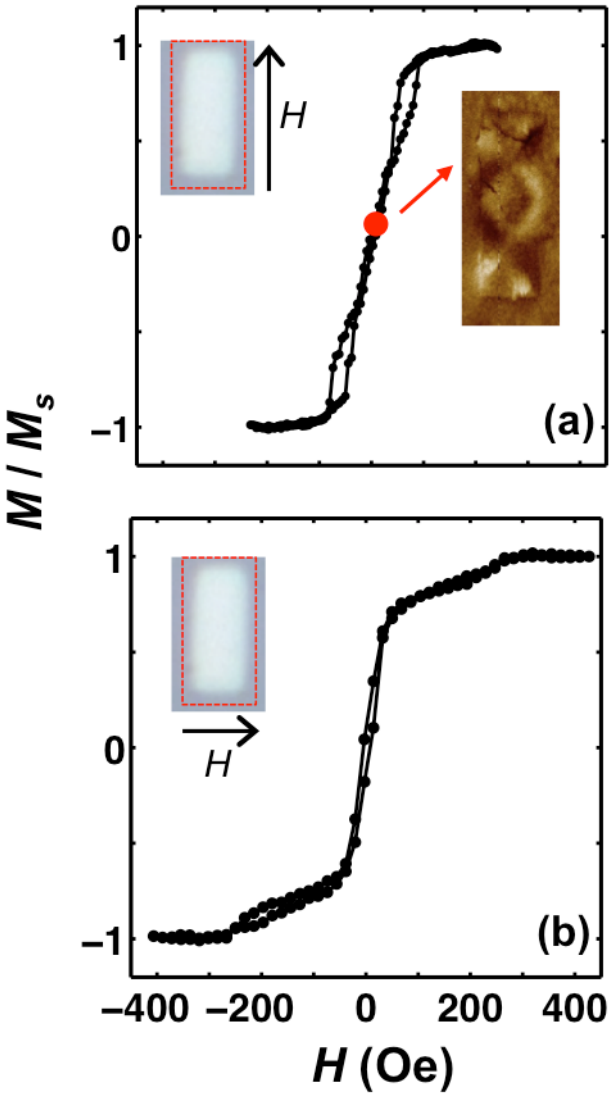

Figure 8: Hysteresis loops measured on the 2 µm x 5 µm FEBID Co structure for different applied field directions; the left part insets display the applied field direction; in (a) the field was applied parallel to the long axis of the structure, and in (b) the field was applied along the short axis of the structure. The inset on the right hand side of Figure (a) shows a magnetic force microscopy image taken at remanence after previously saturating the structure along the long axis.

in magnetostatic energy of this hard axis state also leads to the fact that a relatively large applied field of around 250 Oe is needed to saturate the sample, which can be seen in Figure 8 (b).

This tendency of increased and anisotropic hysteresis in smaller structures with larger geometric anisotropy is also visible in Figure 9. This Figure displays hysteresis loops measured on the 5 µm x 1 µm structure upon applying the external magnetic field in the direction of the long (Figure 9 (a)) and short (Figure 9 (b)) axes of the structure, respectively. Again, the left-hand insets in both Figures represent the selected ROI. For this sample, we now observe a non-vanishing magnetization value at remanence for the easy axis, i.e. for the externally applied field parallel to the long axis of the structure. The main reason of this is the further increased difficulty of the system to form a complete flux closure structure due to the high cost of the exchange energy associated with multi-domain states in structures of reduced size. The inset on the right-hand side of Figure 9 (a) shows a schematic of the possible domain structure in remanence after applying the field parallel to the long axis. Experimentally, the hysteresis loop shows a plateau-like structure at remanence that arises from the energetic stability of this multi-domain state. Overall, a much lager hysteresis effect is visible in this structure due to the decreased ability to form multiple domain states easily that would otherwise minimize the magnetostatic energy. When the external field is applied along the short axis, a small opening of the hysteresis is visible as well, which arises from the parallel alignment of the edge magnetization states with the applied field as seen in the inset on the right-hand side of Figure 9 (b). While this alignment has an increased magnetostatic energy at zero field, it is initially favored during the hysteresis loop cycle by the originally applied field. Subsequently, the activation energy to suppress this state in remanence is too high for this narrow sample shape, so that it persists and causes a small hysteresis effect.

The magnetic data in Figures 7, 8, and 9 indicate that all the FEBID fabricated elements display the ideal behavior of magnetic micro-sized elements that are made from magnetic films that have uniform thickness, uniform magnetic properties and a strong intra-layer exchange coupling resulting in a collective magnetic response [32-34]. Thus, under the conditions used here, FEBID Co of uniformly high quality gets deposited with uniform rates over relevant areas of several microns in size. This is, of course, a most crucial precondition for reliable structure and device fabrication based on FEBID.

In order to demonstrate the capability of FEBID to fabricate more complex shapes and functional structures, we have also fabricated Co domain wall conduits. Specifically, Figure 10 (a) shows a SEM image of a Co domain wall conduit with an injection pad, while Figure 10 (b) shows Co domain wall conduit elements with different aperture angles, namely 10°, 20° and 30°. Similar domain wall conduits have been proposed and applied as suitable devices for trapping and manipulating magnetic nanoparticles or biological entities attached to magnetic nanoparticles [35]. In order to check the functionality of these structures, we have measured the magnetic properties of these domain wall conduits by MFM at remanence after applying the field along the

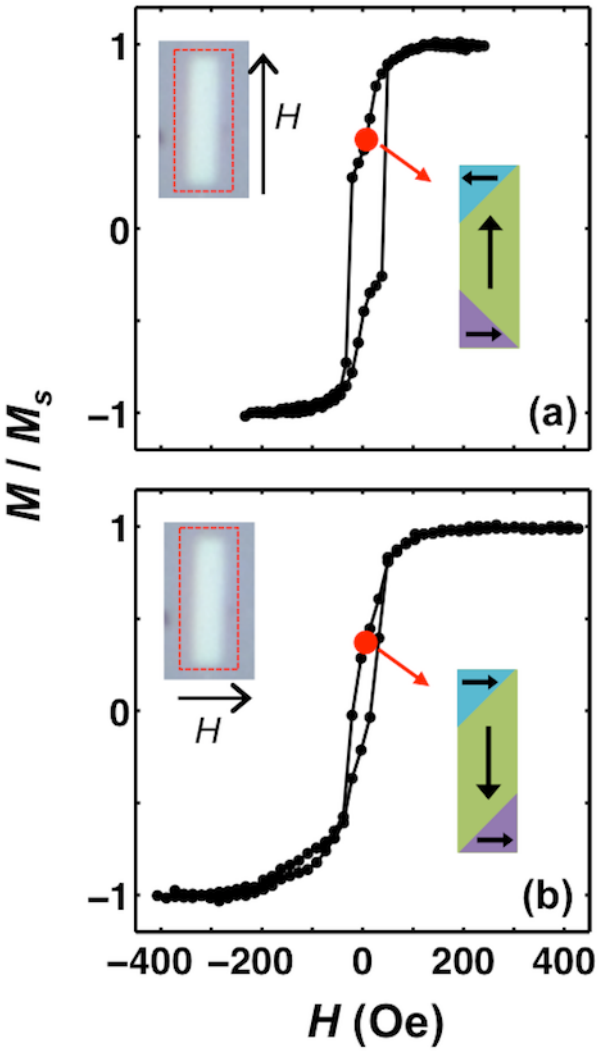

Figure 9: Hysteresis loops measured on the 1 µm x 5 µm FEBID Co structure for different applied field directions; the left part insets display the applied field direction; in (a) the field was applied parallel to the long axis of the structure, and in (b) the field was applied along the short axis of the structure. The insets on the right hand sides of both Figures represent schematics of the magnetic domain states in remanence after previously saturating the structure parallel to the long axis (a) and parallel to the short axis (b).

short axis (Figure 10 (c)), as well as the long axis of the overall structure (Figure 10 (d)). In the first case, the MFM image visualizes the occurrence of charged domain wall formation at the corners of the structures, which results from magnetic moments pointing in the same direction in all the stripes (Figure 10 (e)). Following the contrast that is observed in the MFM measurements, the top corners contain head-to-head domain walls, while the bottom corners are populated with tail-to-tail domain walls. Please note that while Figure 10 (e) provides a schematic of the domain configuration that explains the dominating contrast in the MFM measurement (Figure 10 (c)), the actual detailed domain structure in the experiment is more complex. Specifically, the end segments of the domain wall conduits do not exhibit the nearly uniform magnetization state that is found in the center of the overall structure. These deviations from the simple picture shown in Figure 10 (e) are induced by the magnetostatic self-energy of the structures.

In the remanent state after saturating the structure parallel to the long axis of the conduit (Figure 10 (d)), no domain wall can be detected, which comes from the fact that the magnetization builds up a flux closure structure (Figure 10 (f)). So while domain walls are also present in this case, their structure is such that the flux is contained inside the conduit. Therefore, no magnetic field can be detected by the MFM outside the sample at these domain walls. Considering the schematics in Figure 10 (f), one should expect an MFM contrast at the end points of the domain wall conduits in Figure 10 (d). However, just as already discussed in conjunction with Figure 10 (e), Figure 10 (f) shows a simplified physical picture to explain the dominating experimental contrast mechanism, but does not necessarily apply to fine details of the magnetic structure at the end points. In any case, from these MFM results it is clear that the conduits have two remanent states that are fundamentally different. One creates a sizable magnetic field and thus attracts magnetic nano-particles, while the other one is nearly field free and thus invisible to magnetic entities, i.e. these conduits can be turned on and off. Moreover, we were able to displace domain walls in conduits with injection pads by applying an adequate external field sequence. All these tests demonstrate that the FEBID fabricated structures are functional and therefore suitable to displace magnetic domain walls reliably via field or current sequences for the purpose of magnetic nano-particle transport [36].

Despite the successful fabrication of functional structures, the magnetic images in Figure 10 reveal one of the key technical difficulties of FEBID. If one looks very closely at these images, one can see that the

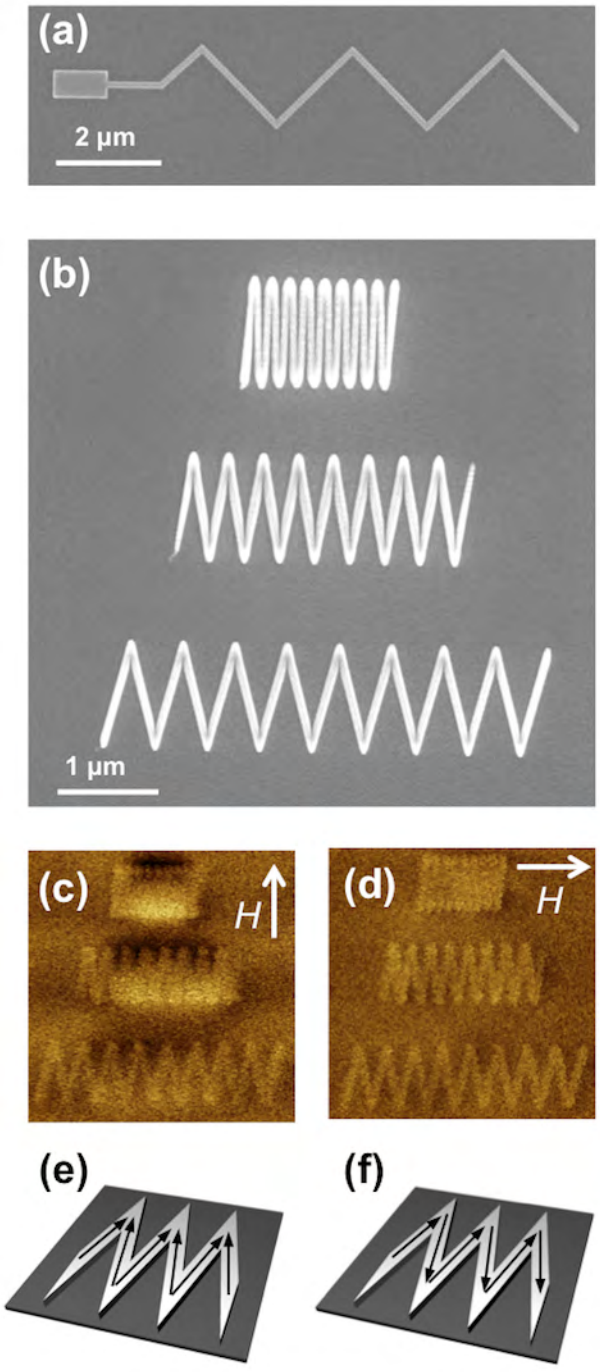

Figure 10: FEBID Co domain wall conduit structures: (a) scanning electron microscope image of a conduit structure with a domain wall injection pad. (b) shows a scanning electron microscope image of conduit structures with different aperture angle, which are 10°, 20° and 30° from top to bottom. (c) and (d) show magnetic force microscope images of the structures, shown in (b), taken at remanence after saturating the structure along the short axis (c) and parallel to the long axis (d) of the entire structure. (e) and (f) represent schematics of the ideal magnetization states at remanence after saturation along the short axis (e) and parallel to the long axis (f) of the entire structure.

surrounding regions of the actual device component structures also show a magnetic signal. This is due to the unintended halo-like growth around the intended functional structures. This halo can be the result of autocatalytic growth, surface activation or secondary electrons generated by highly energetic backscattered electrons. While there are reports in the literature that seem to demonstrate that these halo-like structures have low Co concentration and therefore should not affect the magnetic functionality of the intended structures and devices [20], we have recently shown that this is not necessarily the case and that functionalities can indeed be modified by the existence of these unintended halo deposits [37]. Specifically, we demonstrated for densely packed Co nanopillars structures that the existence of secondary halo-deposits results in magnetic exchange coupling in between neighboring nanopillars. We have also demonstrated a pathway to eliminate this unintended deposit and correspondingly the halo-induced functional modifications by means of a suitable post deposition treatment process. Hereby, a Xe-ion beam was used to irradiate the as-deposited structures and eliminate the halo by means of broad beam ion milling. Other groups also investigated the possibility to eliminate this type of halo by means of ion milling, using Ga- or Ar-ions [26,38]. As an example of the efficiency of this process, we show a set of six Co nanowires separated by different distances between them, namely 30, 60, 90, 120 and 150 nm, which has been irradiated by different Xe-ion doses. Otherwise, the fabrication parameters for all these structures were identical: electron beam voltage 25 kV, electron beam current 2.7 nA, dwell time 1 µs, pitch size 5 nm and a total deposition time per nanowire of 2 s. Figure 11 (a) shows SEM images of these nanowires as deposited, while Figures 11 (b) and (c) show the same type of structure after 60 mC/cm^2 and 85 mC/cm^2 of Xe-ion beam exposure, respectively. Hereby, we utilized a Xe-ion beam energy of 1 keV. The insets in Figure 11 show cross-sectional scanning transmission electron microscopy (STEM) images of the nanowires that are separated by 150 nm for each of the post treatment cases. In the case of the as-deposited structures (Figure 11 (a)), it is actually difficult to see the halo structure in the top view SEM image due to the fact that it forms as a continuous flat film layer. However, the STEM image reveals its presence clearly as a 4-5 nm thick film in the area surrounding the intended deposit. After Xe irradiation with a dose of 60 mC/cm^2 (Figure 11 (b)), the SEM image, as well as the STEM image, shows a considerable decrease of the halo material. Upon increasing the Xe ion dose, the halo reduces even further up to a point, at which it

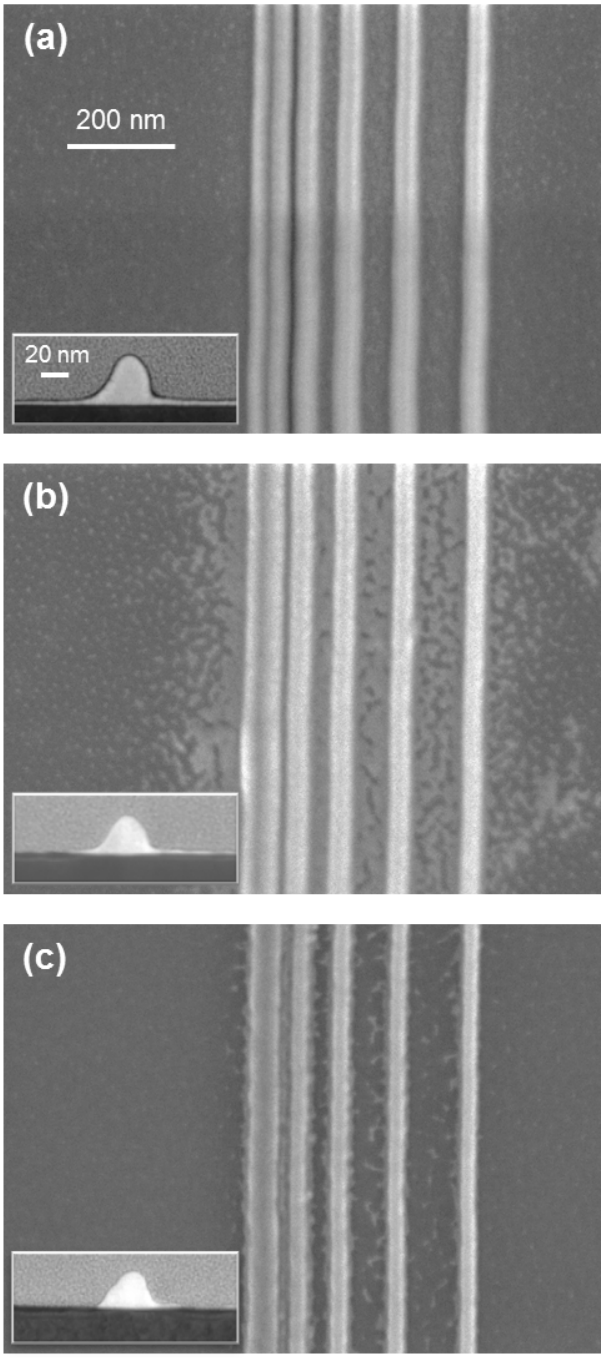

Figure 11: FEBID structures in conjunction with the Xe-ion post-treatment process; (a)-(c) show scanning electron microscopy images of 6 Co wires with different distances in between them, namely 30, 60, 90, 120 and 150 nm. While (a) is taken after deposition only, (b) and (c) correspond to images taken after 60 mC/cm^2 and 85 mC/cm^2 of Xe-ion beam exposure. The inset Figures show scanning transmission electron microscope images of a cross section of an individual wire each, after deposition (inset in (a)), and after additional Xe beam exposure of 60 mC/cm^2 (inset in (b)) and 85 mC/cm^2 (inset in (c)). Figures (a) and (c) reprinted with permission from E. Nikulina, O. Idigoras, J. M. Porro, P. Vavassori, A. Chuvilin and A. Berger, Appl. Phys. Lett. **103**, 123112 (2013). Copyright 2013, AIP Publishing LLC.

nearly disappears as shown by the structures that were irradiated by the 85 mC/cm^2 Xe ion dose (Figure 11 (c)). Given the fact that the intended deposit structure is not strongly altered by these Xe-ion doses, it is actually possible to use FEBID fabrication plus Xe milling post-treatment for the fabrication of functional Co nano-structures and devices.

As previously mentioned, FEBID is a powerful technique that is suitable for the fabrication of 3-dimensional structures. However, up to now there are only few works that show the ability to fabricate 3D magnetic nano-structures by means of FEBID [20,21]. To demonstrate the viability of 3-dimensional fabrication and to complement the already existing work on this subject, Figure 12 shows SEM images of a Co spiral array that was observed at an angle of 45° with respect to the surface plane as well as a top view image of the same structure. These specific structures were fabricated by using an electron beam energy of 5 keV and electron beam current of 690 pA. It should also be mentioned that below the main spirals, a parasitic deposit can be observed in the SEM images. It is very difficult to avoid the initial deposition of such parasitic deposits on solid substrates for 3 dimensional structures, because electrons are bound to reach the substrate during the deposition process. However, we envision that these parasitic deposits can be reduced by adequately managing the deposition conditions or they can be subsequently removed by post deposition treatments.

4 Discussion

This work gives an illustration of the viability of FEBID to fabricate magnetic nano- and micro-structures and it demonstrates that by a combination of MOKE microscopy and MFM, one is able to analyze size and shape effects onto the magnetization state and reversal of individual magnetic Co structures. With the help of our magnetic and thus functional study, we are able to demonstrate that FEBID Co of uniformly high quality, i.e. uniform thickness, smooth surface and high purity, can be deposited with uniform rates over areas of several microns in size. Therefore, a most crucial ingredient of reliable structure and device fabrication by means of FEBID is established. Furthermore, we have shown the suitability of FEBID to fabricate functional and complex 3-dimensional magnetic structures. The issue of unintended secondary deposits in FEBID is discussed, and a Xe-ion milling post-treatment for its removal is proposed and demonstrated as a successful pathway towards the fabrication of functionally independent magnetic nano-structures.

Acknowledgments: We acknowledge financial support from FEI Company (Netherlands), the Basque Government under the Etortek Program Contract No. IE11-304 and Projects PI2012-47 and CTP11-P14, as well as the Spanish Ministry of Science and Education under Project No. MAT2012-36844. O.I. and J.M.P. acknowledge the Basque Government for Fellowships (Nos. BFI09-284 and BFI09-289, respectively).

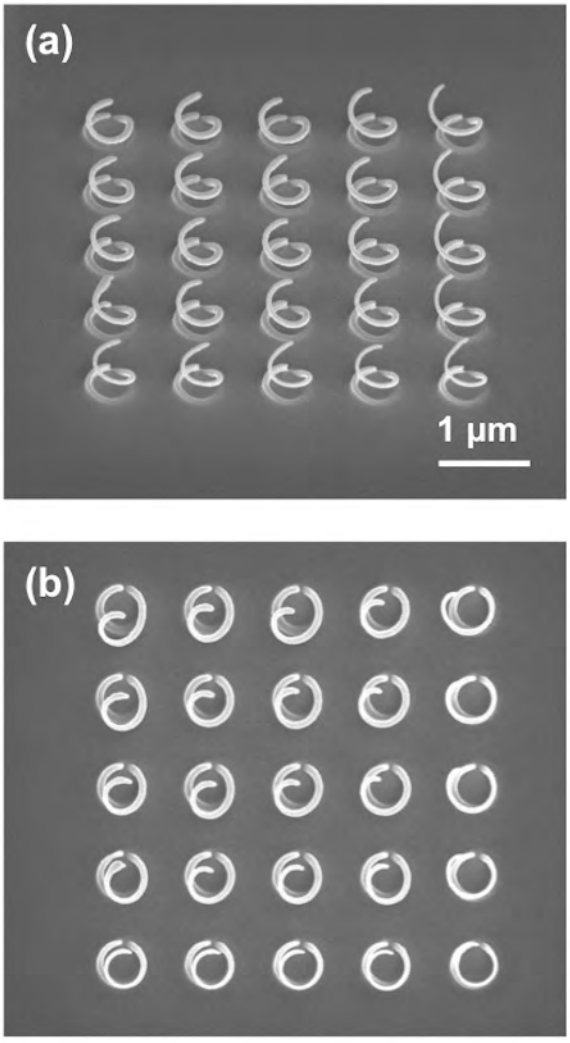

Figure 12: Scanning electron microscopy images of an array of FEBID Co spirals; (a) shows an image taken at an angle of 45° with respect to the surface plane and (b) shows a top view image for the same structure.

References

[1] Piramanayagam S. N., Srinivasan K., Recording media research for future hard disk drives, J. Magn. Magn. Mater., 2009, 321, 485–494.

[2] Miller M. M., Prinz G. A., Cheng S.-F, Bounnak S., Detection of a micron-sized magnetic sphere using a ring-shaped anisotropic magnetoresistance-based sensor : A model for a magnetoresistance-based biosensor, Appl. Phys. Lett., 2002, 81, 2211.

[3] Allwood D. A., Xiong G., Faulkner C. C., Atkinson D., Petit D., Cowburn R. P., Magnetic domain-wall logic, Science, 2005, 309, 1688–92.

[4] Repain V., Jamet J.-P., Vernier N., Bauer M., Ferré J., Chappert C., Gierak J., Mailly D., Magnetic interactions in dot arrays with perpendicular anisotropy, J. Appl. Phys., 2004, 95, 2614.

[5] Berger A., Lengsfield B., Ikeda Y., Determination of intrinsic switching field distributions in perpendicular recording media, J. Appl. Phys., 2006, 99, 08E705.

[6] Berger A., Supper N., Ikeda Y., Lengsfield B., Moser A., Fullerton E. E., Improved media performance in optimally coupled exchange spring layer media, Appl. Phys. Lett., 2008, 93, 122502.

[7] Hovorka O., Liu Y., Dahmen K. A., Berger A., Simultaneous determination of intergranular interactions and intrinsic switching field distributions in magnetic materials., Appl. Phys. Lett., 2009, 95, 192504.

[8] Fernández-Pacheco A., De Teresa J. M., Szkudlarek A., Córdoba R., Ibarra M. R., Petit D., O'Brien L., Zeng H. T., Lewis E. R., Read D. E., et al. Magnetization reversal in individual cobalt micro- and nanowires grown by focused-electron-beam-induced-deposition, Nanotechnology, 2009, 20, 475704.

[9] Breitkreutz S., Kiermaier J., Vijay Karthik S., Csaba G., Schmitt-Landsiedel D., Becherer M., Controlled reversal of Co/Pt dots for nanomagnetic logic applications, J. Appl. Phys., 2012, 111, 07A715.

[10] Nikulina E., Idigoras O., Vavassori P., Chuvilin A., Berger A., Magneto-optical magnetometry of individual 30 nm cobalt nanowires grown by electron beam induced deposition, Appl. Phys. Lett., 2012, 100, 142401.

[11] Neumann A., Thönnissen C., Frauen A., Hesse S., Meyer A., Oepen H. P., Probing the magnetic behavior of single nanodots, Nano Lett., 2013, 13, 2199.

[12] Chaves-O'Flynn G. D., Vanden-Eijnden E., Stein D. L., Kent A. D., Energy barriers to magnetization reversal in perpendicularly magnetized thin film nanomagnets, J. Appl. Phys., 2013, 113, 023912.

[13] Ralph D. C., Stiles M. D., Spin transfer torques, J. Magn. Magn. Mater., 2008, 320, 1190–1216.

[14] Maruyama T., Shiota Y., Nozaki T., Ohta K., Toda N., Mizuguchi M., Tulapurkar A. A., Shinjo T., Shiarishi M., Mizukami S., et al. Large voltage-induced magnetic anisotropy change in a few atomic layers of iron, Nat. Nanotechnol., 2009, 4, 158–161.

[15] Parkin S. S. P., Hayashi M., Thomas L., Magnetic domain-wall racetrack memory, Science, 2008, 320, 190–194.

[16] van Dorp W. F., Hagen C. W., A critical literature review of focused electron beam induced deposition, J. Appl. Phys., 2008, 104, 081301.

[17] Utke I., Moshkalev S., Russel P., Nanofabrication using focused ion and electron beams: principles and applications; Oxford University Press: New York, 2012.

[18] Huth M., Porrati F., Schwalb C., Winhold M., Sachser R., Dukic M., Adams J., Fantner G., Focused electron beam induced deposition: A perspective, Beilstein J. Nanotechnol., 2012, 3, 597–619.

[19] van Dorp W. F., van Someren B., Hagen C. W., Kruit P., Crozier P., Approaching the resolution limit of nanometer-scale electron beam-induced deposition, Nano Lett., 2005, 5, 1303–7.

[20] Lau Y. M., Chee P. C., Thong J. T. L., Ng V., Properties and applications of cobalt-based material produced by electron-beam-induced deposition. J. Vac. Sci. Technol., A 2002, 20, 1295.

[21] Fernández-Pacheco A., Serrano-Ramón L., Michalik J. M., Ibarra M. R., De Teresa J. M., O'Brien L., Petit D., Lee J., Cowburn R. P., Three dimensional magnetic nanowires grown by focused electron-beam induced deposition, Sci. Rep., 2013, 3, 1492.

[22] Serrano-Ramón L., Córdoba R., Rodríguez L. A., Magén C., Snoeck E., Gatel C., Serrano I., Ibarra M. R., De Teresa J. M., Ultrasmall functional ferromagnetic nanostructures grown by focused electron-beam-induced deposition, ACS Nano, 2011, 5, 7781–7787.

[23] Belova L. M., Dahlberg E. D., Riazanova A., Mulders J. J. L., Christophersen C., Eckert J., Rapid electron beam assisted patterning of pure cobalt at elevated temperatures via seeded growth, Nanotechnology, 2011, 22, 145305.

[24] Boero G., Utke I., Bret T., Quack N., Todorova M., Mouaziz S., Kejik P., Brugger J., Popovic R. S., Hoffmann P., Submicrometer hall devices fabricated by focused electron-beam-induced deposition, Appl. Phys. Lett., 2005, 86, 042503.

[25] Utke I., Michler J., Gasser P., Santschi C., Laub D., Cantoni M., Buffat, P. A., Jiao C., Hoffmann P., Cross section investigations of compositions and sub-structures of tips obtained by focused electron beam induced deposition, Adv. Eng. Mater., 2005, 7, 323–331.

[26] Serrano-Ramón L., Fernández-Pacheco A., Ibarra M. R., Petit D., Cowburn R. P., Tyliszeczak T., De Teresa J. M., Modification of domain-wall propagation in Co nanowires via Ga^+ irradiation, Eur. Phys. J. B, 2013, 86, 97.

[27] Allwood D. A., Xiong G., Cooke M. D., Cowburn R. P., Magneto-optical Kerr effect analysis of magnetic nanostructures, J. Phys. D Appl. Phys., 2003, 36, 2175–2182.

[28] Zeng H. T., Read D., O'Brien L., Sampaio J., Lewis E. R., Petit D., Cowburn R. P., Asymmetric magnetic NOT gate and shift registers for high density data storage, Appl. Phys. Lett., 2010, 96, 262510.

[29] Schäfer R., Handbook of magnetism and advanced magnetic materials. Vol. 3: Novel techniques for characterizing and reparing samples. Part 5.; Kronmüller H., Parkin S. S., Eds.; John Wiley & Sons, Ltd, Chichester, 2007.

[30] Idigoras O., Vavassori P., Porro J. M., Berger A., Kerr microscopy study of magnetization reversal in uniaxial Co-films, J. Magn. Magn. Mater., 2010, 322, L57–L60.

[31] Hartmann U., Magnetic force microscopy, Annu. Rev. Mater. Sci., 1999, 29, 53–87.

[32] Rave W., Hubert A., Magnetic Ground State of a Thin-Film Element, IEEE Trans. Magn., 2000, 36, 3886.

[33] Hankemeier S., Frömter, R., Mikuszeit N., Stickler D., Strillrich H., Pütter S., Vedmedenko E. Y., Oepen, H. P., Magnetic Ground State of Single and Coupled Permalloy Rectagle, Phys. Rev. Lett. 2009, 103, 147204.

[34] Xie K., Zhang X., Lin W., Zhang P., Sang H., Phys. Rev. B, 2011, 84,054460.
[35] Donolato M., Torti A., Kostesha N., Deryabina M., Sogne E., Vavassori P., Hansen M. F., Bertacco R., Magnetic domain wall conduits for single cell applications, Lab Chip, 2011, 11, 2976–83.
[36] Vavassori P., Metlushko V., Ilic B., Gobbi M., Donolato M., Cantoni M., Bertacco R., Domain wall displacement in Py square ring for single nanometric magnetic bead detection, Appl. Phys. Lett., 2008, 93, 203502.
[37] Nikulina E., Idigoras O., Porro J. M., Vavassori P., Chuvilin A., Berger A., Origin and control of magnetic exchange coupling in between focused electron beam deposited cobalt nanostructures. Appl. Phys. Lett., 2013, 103, 123112.
[38] De Teresa J.M., Córdoba R., Arrays of Desenly Packed Isolated Nanowires by Focused Beam Induced Deposition Plus Ar+ Milling, ACS Nano, 2014, 8, 3788-95.